Materials and Design 87 (2015) 380–385

Contents lists available at ScienceDirect

Materials and Design

journal homepage: www.elsevier.com/locate/jmad

In situ heat treatment in selective laser melted martensitic AISI 420 stainless steels

P. Krakhmalev [a,*], I. Yadroitsava [b], G. Fredriksson [a], I. Yadroitsev [b]

[a] Karlstad University, Department of Engineering and Physics, Karlstad SE-651 88, Sweden
[b] Central University of Technology, Free State, Department of Mechanical and Mechatronic Engineering, Private Bag X20539, Bloemfontein 9300, South Africa

ARTICLE INFO

Article history:
Received 17 June 2015
Received in revised form 6 August 2015
Accepted 10 August 2015
Available online 12 August 2015

Keywords:
Microstructure
Martensitic stainless steel
In situ heat treatment
Selective laser melting

ABSTRACT

The article explores an evolution of a microstructure in AISI 420 martensitic stainless steel during selective laser melting. Several upper layers had hardness of 750 HV and contained 21 ± 12 vol.% austenite phase. The final bulk microstructure consisted of thermally decomposed martensite with hardness of 500–550 HV and unusually high, 57 ± 8 vol.%, amount of austenite. Obtained results indicate that during manufacturing a partitioning and austenite reversion took place, owing to the thermal cycling of the inner regions during manufacturing. Numerical simulation was found plausible to analyze and explain thermally activated processes that occurred in situ. Results of numerical simulation of the thermal cycles in dependence on the processing parameters suggested a possibility to control the thermal processes by variation of the laser energy input.

1. Introduction

Dynamic growth in metal additive manufacturing during last years is driven by requirements of modern industries to increase product performance by a combination of enhanced properties and sophisticated design along with a decreased material consumption. The use of industrial metal additive manufacturing systems in automotive, aerospace and medical markets grows strongly [1]. Additive manufacturing methods, and particularly selective laser melting (SLM), are widely accepted for fabrication of parts with complex geometries and inner functional structures [1,2]. These advantages are attractive for the high-tech industries, but high demands on microstructure and properties in the final product often limit direct applicability of as built SLM products. General progress was obtained when a relevant manufacturing strategy was developed. This strategy includes a multi-level hierarchical approach to minimize manufacturing defects like porosity, cracks and deformation during processing. A high integrity of the final 3D object can be achieved by using the optimal strategy and process parameters [3–7]. Nevertheless, due to the complete remelting of the powder material and the rapid solidification, a microstructure which is anisotropic and different from the conventional is usually observed in SLM parts.

SLM is a process involving heating and cooling cycles, which initiate in situ diffusion processes similar to tempering, relaxation or precipitation which in turn affect the microstructure in the already solidified inner regions. Understanding of these processes and an ability to control them is an advantage that can provide predictable and tailored combinations of microstructure and properties in SLM objects. This investigation is focused on numerical modeling of the thermal cycling and experimental investigation of the in situ microstructural evolution in AISI 420 stainless steel during SLM.

2. Materials and method

Spherical gas-atomized powder AISI 420 (in wt.%: Fe-bal., Cr—13.2, Mn—0.73, Si—0.66, C—0.39, O—0.039, P—0.010, S—0.007) supplied by Sandvik Osprey Ltd. was used. The volume equivalent sphere diameters were d_{10} = 8.2 μm, d_{50} = 22.5 μm and d_{90} = 37.6 μm. SLM experiments were carried out using a single-mode continuous-wave Ytterbium fiber laser operating at 1075 nm wavelength (IPG Photonics Corp.) in a protective atmosphere of nitrogen. The laser beam had a TEM_{00} Gaussian profile, 70 μm spot size, and 200 W maximum power. For microstructure assessment, cube-shape 10 × 10 × 10 mm specimens were manufactured using a rescanning strategy: each layer was scanned twice by the laser. In the first scan, a laser beam melts a powder layer with a certain hatch distance and then, without deposition of any new powder, the laser beam shifts and rescans the surface again, in the same direction but between the previously formed tracks, Fig. 1. After that, the scanning direction was changed to the orthogonal and next layer was manufactured. This rescanning strategy significantly improves surface quality and minimizes porosity in the final 3D SLM objects [8,9]. The laser power of 60 W, 120 mm/s scanning speed and 120 μm hatch distance were used as manufacturing process parameters. Thickness of the deposited powder layer was 40 μm.

Microstructural characterization of as built specimens was done by means of X-ray diffraction, optical and electron microscopy. Specimens

* Corresponding author.
E-mail address: pavel.krakhmalev@kau.se (P. Krakhmalev).

http://dx.doi.org/10.1016/j.matdes.2015.08.045
0264-1275/

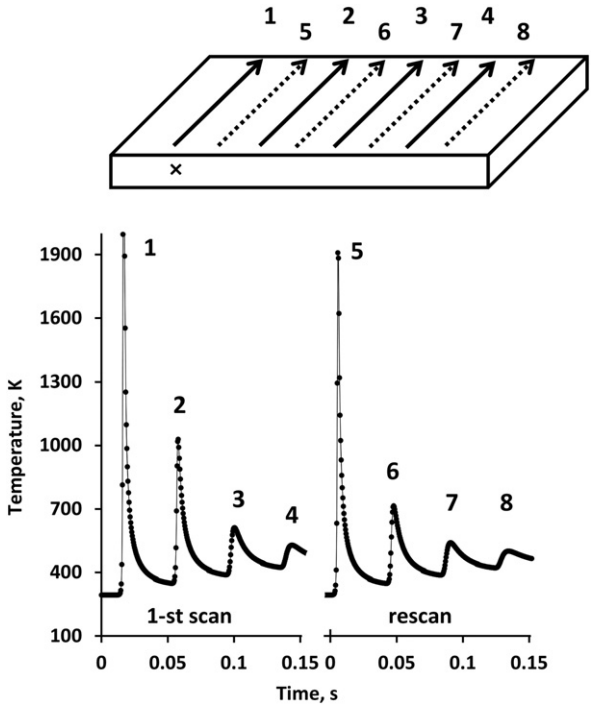

Fig. 1. Schematic of the used manufacturing strategy and an example of thermal cycles estimated in the point (×) during manufacturing. Points 1, 2, 3, and 4 correspond to the first scan and, points 5, 6, 7, and 8 to the re-scan at manufacturing of the same layer. Arrows indicate the laser movement direction.

were cut to transverse cross sections, ground and mirror-like polished with 1 μm diamond paste. A standard Kalling's №2 reagent was used to etch specimens for microscopy. For the EBSD observations, a colloidal silica was used for the final step of surface preparation. Vickers microhardness was measured using Buehler Micromet 5104 with an indentation load of 300 g. Scanning electron microscopy (SEM) was carried out with LEO 1350 FEG–SEM and analytical SEM Hitachi SU70, both operated at 20 kV. Orientation imaging microscopy was performed using an electron back-scattering diffraction (EBSD) system from HKL Technology. X-ray diffraction (XRD) phase analysis was conducted using Cr-Kα radiation in a Seifert XRD 3000 PTS X-ray diffractometer, operating at 40 kV and 35 mA, the spot was 2 mm in diameter. Measurements were done on the polished cross-section to investigate amount of austenite in the inner regions and on the as built top surface to detect amount of austenite in the top layers. The volume fraction of the fcc phase was calculated accordingly to the standard ASTM E975-13 procedure.

3. Results and discussion

3.1. Numerical modeling of thermal cycles

In order to interpret and explain the evolution of microstructure during the in situ heat-treatment at manufacturing, numerical simulations were done. The main aim of the modeling was to estimate temperatures in the bulk material and to compare the results with the experimentally observed remelting depth. As mentioned earlier, for the manufacturing of 3D samples a rescanning strategy was applied. A complexity of this strategy is that at the first scan, the laser remelted the deposited powder layer, while during re-scanning laser remelts already solidified material. Therefore, as a first attempt, for evaluation of temperature fields, the laser-powder interaction was disregarded. Modeling was carried out using time-dependent COMSOL module "Heat Transfer in Solids" (COMSOL, Inc.). In the used simulation, the laser was modeled as a moving energy source with a Gaussian energy distribution. The laser spot was circular, 70 μm in diameter. Similarly to [10] the conductive mode of heat transport was modeled, convection in liquid and radiation energy losses were ignored since they have a minor contribution in the energy dissipation. The temperature-dependent material properties were found in the Comsol material library, 2015. A temperature-dependent specific heat capacity was selected with respect to the latent heat of phase transitions. The effective thermal conductivity of a liquid metal was imposed taking into account the heat transfer due to flows. In the finite element model, the 5 mm long scans were simulated at the top surface of a rectangular steel block. The block was 1 mm thick with the top surface 6 × 2 mm. The scan length of was large enough to establish a stationary process of laser melting. The element mesh in the scanned region was 0.5 μm. At the top surface a convective heat transfer was modeled since SLM is done in a protective gas atmosphere. All the other surfaces of the metal block were assumed to be thermally insulating. The chamber temperature was maintained at 293 K. A detailed description of this model including equations and relevant references could be found in [7]. To validate the model, the experimentally observed geometrical characteristics of the molten pool were compared with the modeling results. It was found that for the same set of laser spot size, hatch distance, laser speed and, laser power the geometrical characteristics of the molten pool were in a good agreement with the experiment. Therefore, the model was assumed plausible for an estimation of thermal cycling in situ occurred in the SLM fabricated specimen of AISI 420 stainless steel.

The thermal cycles at depths of 0, 40, 80, 120, and 160 μm were calculated, Fig. 2. The selection of depths was based on microscopy observations and the depths correspond to the central points of the first tracks in five fabricated layers. The thermal cycles at the depth of 0 μm correspond to thermal effects in the center of the first track, during the build-up of the top layer itself, Fig. 1. The thermal history in the previous layer, at a depth of 40 μm, consists of thermal cycles when this layer was built-up itself and thermal effects from when the subsequent layer was built. Thus, the whole Fig. 2 represents the calculated thermal history at the depth of five fabricated layers. The calculations showed that simulation of more laser scans or to larger depths is not reasonable since the estimated temperatures would be lower than the critical M_s temperature and, therefore, assumed to have no significant influence on the microstructure.

3.2. Microstructural characterization

The characterization of microstructures showed that the SLM specimen of AISI 420 stainless steel has a pore-free microstructure without primary carbides. Microscopy, microhardness profile measurements and XRD analysis showed that the upper layers of the specimen have a microstructure of fresh martensite with a maximum hardness of 750 HV to depths of about 100–120 μm. XRD detected 21 ± 12 vol.% of retained austenite in the top surface layers. The inner regions showed an appearance similar to tempered martensite and a hardness of 500–550 HV, with a high content of austenite, 57 ± 8 vol.%, as revealed by XRD.

In the annealed condition this steel commonly contains primary Cr-rich carbides. However, no primary carbides were detected by SEM or XRD in the microstructure after SLM. This could be a result of the repeated remelting of the material that leads to complete dissolution of the primary carbides, together with rapid solidification which prevents precipitation of them. Similar carbide-free structures were reported for laser treated [11] and welded [12] AISI 420 stainless steel. According to the CCT diagram presented in [13], at cooling rates of 2°/s or higher, the primary carbides are not formed at continuous cooling. Numerical modeling of the heating–cooling cycle showed, see Fig. 1, that the cooling rates at SLM were substantially higher than that threshold of 2°/s. Similarly, quite high cooling rates were reported for direct laser fabricated AISI 420 [14] and SLM austenitic stainless [15] steel.

At SLM of steels, the austenite formed at rapid solidification after remelting has a morphology of elongated colonies of cellular cells. This type of microstructure has been investigated thoroughly for instance

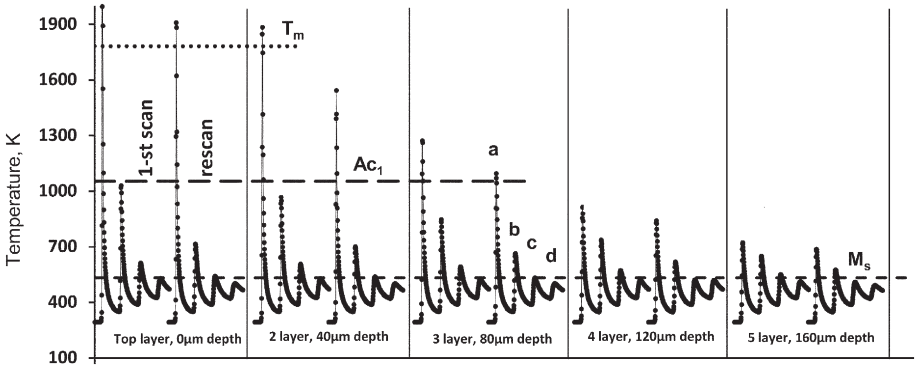

Fig. 2. Numerical simulation of thermal cycling at different depths during laser melting of AISI 420 steel. The insert illustrates modeled temperatures and time after 1-st scan at the top layer, 0 μm depth. Axis X represents an order of the scans and the layers during manufacturing.
Critical points adopted from [13].

in the austenitic stainless AISI 316L steel and other metallic materials manufactured by SLM [3,16,17]. In steels, TEM and EBSD investigations have shown that the cells in a single colony were coherent, i.e. have the same crystallographic orientation, and grew along the <100> crystallographic direction [16,18]. Boundaries between cells are thick dislocation structures, different from the regular high-angle grain boundaries [3]. This type of cellular microstructures has been observed in laser or electron beam manufactured metals [17,19]. In AISI 420 steel, the austenite–martensite phase transformation takes place after cooling below the M_s temperature. The martensite phase has a distinct needle-like morphology, as observed at the top surface of the SLM fabricated specimens, Fig. 3a.

The morphology of the parental austenite phase, the cellular structure and colony boundaries, are still visible on the surface. At martensitic transformation, dislocations from the parental austenite are inherited by the fresh martensite, therefore, the cells were clearly visible in the martensitic structure observed on the top surface of the specimen, Fig. 3a. Notably, the martensitic needles grew through the cells and stopped at the high-angle colony boundaries. The martensitic transformation is a diffusionless and displacive transformation where the fresh martensite has a certain crystallographic relationship with the parental austenite (commonly by Kurdjumov–Sachs relationship $\{111\}_\gamma \parallel \{011\}_\alpha$ and $<10\text{–}1>_\gamma \parallel <11\text{–}1>_\alpha$). The observation that martensite needles have grown through the cell boundaries is therefore additional confirmation of coherency of the parental austenite cells.

Hardness profile measurements showed typical hardness values for fresh martensite of 750 HV to depths down to 100–120 μm. This indicates that there was not any extensive thermally activated decomposition of the martensite in the two–three last deposited layers. Analysis of the thermal history of the three upper layers shows that at manufacturing of the top layer, the temperature reaches above the A_{c1} temperature at depths down to 80 μm. After the last austenitization, by the heat from the first track at rescanning, point "a" in Fig. 2, the steel is rapidly quenched to martensite due to the high cooling rates. The heat from the second track at rescanning, point "b", will heat the material above M_s once, while further tracks will not heat the inner regions higher than the M_s temperature, points "c" and "d".

Theoretically, those temperatures are high enough to initiate diffusional decomposition of fresh martensite. According to [20], carbon can diffuse already at 100–200 °C and segregate at lattice defects. At temperatures of 250–350 °C, the formations of carbides, however, are influenced by alloying elements. Alloying elements like Cr, W, Mo, C and Co impedes precipitation in martensite by affecting the diffusion rate of carbon in the supersaturated solid solution so that martensite can retain up to 450–500 °C [20]. Therefore, enrichment of the steel with alloying elements due to the complete dissolution of the primary carbides could slow down the precipitation. According to the numerical simulation, Fig. 1, a heating–cooling cycle at SLM is very rapid. It is therefore assumed that in the upper layers the martensitic structure remains virtually unaffected due to the higher content of the alloying elements and the kinetic factor.

In principle, analysis of the thermal history in the upper layers suggests that in the SLM objects, a few top layers always have a different thermal history than the inner regions. In the investigated martensitic stainless steel this effect gave a top layer, with higher hardness than the inner regions due to the formation of martensite. For selected applications, a harder surface could be undesirable, therefore, manufacturing-related differences in microstructure and properties in the outer layers should be predicted and taken into account.

Microstructural analysis of inner parts showed a microstructure similar to tempered martensite with a hardness of 500–550 HV. Additionally, unusually high amount of austenite, 57 ± 8 vol.%, was revealed by XRD in the inner parts of the specimen, and these findings qualitatively were confirmed by EBSD, Fig. 4. Red pixels (dark pixels in black and white version) in Fig. 4b correspond to areas in the microstructure identified as fcc iron. Correct quantitative analysis of this data was not possible due to a high amount of not indexed pixels, which could be a

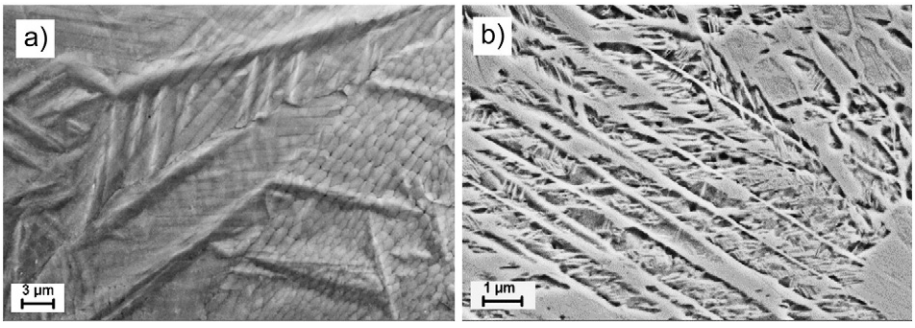

Fig. 3. (a) — Martensitic needles at the top surface, the top surface was not etched or polished, BSE SEM image, (b) — inner regions of thermally affected microstructure of the SLM fabricated AISI 420 steel, etched cross-section, SE SEM image.

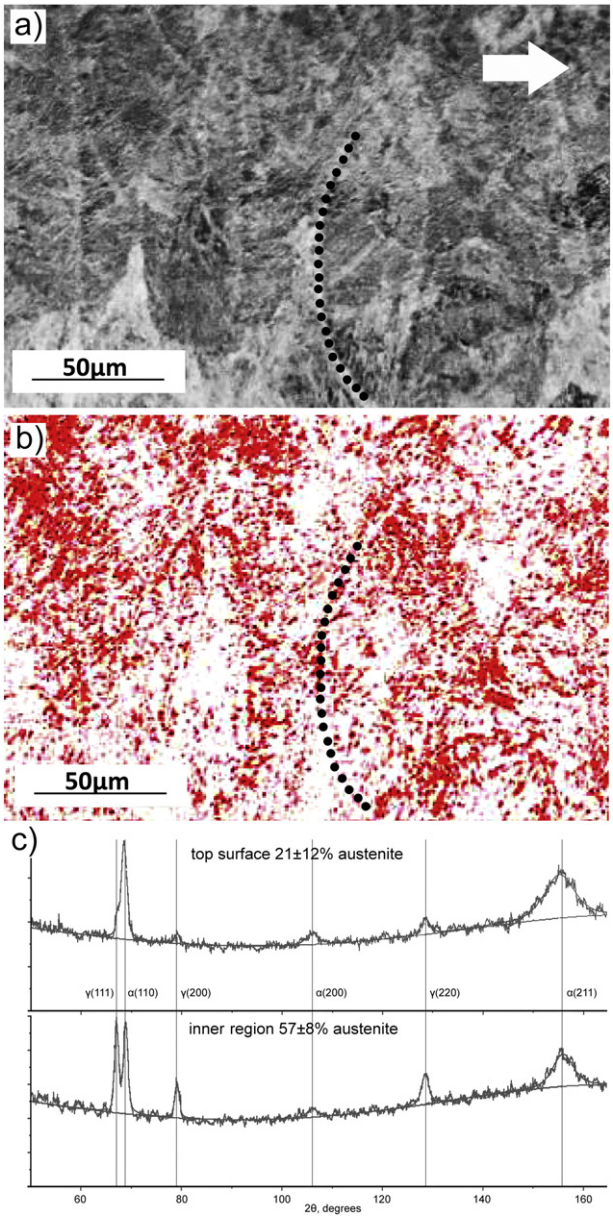

Fig. 4. (a) — SEM image of inner parts of the SLM fabricated AISI 420 steel, (b) — EBSD austenite map of the same region, the building direction is marked by an arrow, an example of the pool boundary marked with a dash line, (c) — XRD pattern obtained from the top surface and the inner region.

result of high residual stresses. Therefore, the quantitative data on the volume fraction of fcc phase was obtained by XRD. Nevertheless, Fig. 4b illustrates a distribution of the fcc phase in the inner parts of the specimen. It is seen that the detected fcc phase distributed quite unevenly.

XRD data presented in Fig. 4c shows peaks of alpha and gamma iron obtained from the top surface and from the inner regions of the specimen. The intensity of gamma peaks substantially different and higher in the inner regions. According to [11] retained austenite in laser surface melted AISI 420 is located at cell boundaries, which is in agreement with the microstructure presented in the SEM picture in Fig. 3b. Here the central regions of a single cell have a morphology of tempered martensite, while the boundaries rather look like retained austenite. Nevertheless, the very high amount of austenite observed in the inner regions cannot be related only to the retained austenite. XRD from the top surface showed presence of 21 ± 12 vol.% austenite, about a half of that measured in the inner regions. As an alternative, the high amounts of austenite in the inner regions could be related to the in situ thermal cycling during manufacturing and, be a result of a partitioning and austenite reversion processes.

Partitioning is a process based on a redistribution of carbon between the martensite and austenite phases at temperatures slightly above M_s. The steel is quenched to temperatures close to M_s and then held for some time at constant temperature to cause carbon redistribution resulting in stabilization of the austenite in the microstructure [21–24]. Usually, this treatment does not lead to formation of new austenite, but to stabilization of the retained austenite already existing at the partitioning temperature. Recently, other regimes for partitioning in AISI 420 have been described [21], where the steel has been quenched down to room temperature and then heated up to 300–500 °C and held for relatively short times to activate diffusion. Substantial austenite reversion, from 8–20 vol.% retained austenite in the as-quenched microstructure up to 40 vol.% has been achieved by this heat treatment for 30 min at 400 °C [21]. This transformation has been explained by a segregation of carbon to martensite–martensite or martensite–retained austenite phase boundaries during quenching. At further heating, the carbon-enriched regions at the martensite–martensite interfaces can revert to the austenite phase. Carbon segregated at the martensite–retained austenite phase boundaries promotes growth of the retained austenite phase [21].

The SLM is a multi-step process involving many quick heating–cooling cycles and therefore, the in situ partitioning process taking place at laser manufacturing has an interrupted character. Numerical simulation of the thermal history in the inner regions, Fig. 2, showed that the temperatures experienced by the inner regions at fabrication were high enough to initiate carbon diffusion. However, because of the short cycle times the diffusion was limited. Apparently, carbon atoms could diffuse short distances and along more defected areas, in this case the cell boundaries. The cell boundaries in the austenite were found to be dislocation structures between coherent cells formed at solidification [3,16], and they were inherited by the martensite, Fig. 3a. Segregation during solidification and further, selective diffusion of carbon, therefore, resulted in the austenite reversion along cell boundaries. This effect is illustrated in Fig. 3b, where the cell boundaries were decorated by the reversed austenite clearly differ from the cell cores. Preferable formation of the austenite phase at cell boundaries can also explain an uneven distribution of the fcc phase observed in the inner regions, Fig. 4. Higher amounts of fcc could locate in regions where cells were finer i.e. contained higher fraction of cell boundaries.

After the quenching and partitioning heat treatment, the AISI 420 steel with high amounts of reversed austenite demonstrates a distinctive combination of high ductility and high ultimate tensile strength, associated with deformation-driven austenite-to-martensite transformation [21]. The results obtained in this investigation of AISI 420 stainless steel showed that partitioning and austenite reversion occurred in situ at SLM manufacturing. The fact that these in situ processes changes microstructure which controls the final properties offers an attractive opportunity to manufacture a component with complex shape and tailored properties in one step, without additional heat treatments afterwards. Additionally, the in situ heat treatment takes place locally in every point, which could eliminate issues related to component thickness and hardenability, the whole bulk, except the top surface, would experience the same heat treatment all the way through. Therefore, a concept of the controllable in situ heat treatment at SLM manufacturing would be realized, if suitable process parameters to control in situ processes were found.

The diffusional character of the in situ processes observed at SLM of AISI 420 steel showed that the control of temperature and heating–cooling time at manufacturing cycles is of highest importance. If the cycle time depends on material properties and is difficult to be manipulated, the temperature can vary substantially with changes of the process parameters. It has been experimentally shown [3] that the key parameters, which influence temperature the most, were laser power

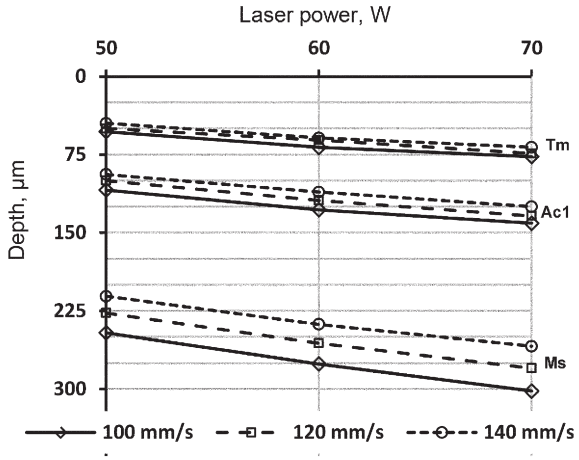

Fig. 5. Simulated isotherms of critical points of the SLM fabricated AISI420 steel, in dependence on the laser power and laser scanning speed.
Critical points adopted from [13].

and laser scanning speed. Additionally, these parameters were easy to control. To estimate the influence of SLM parameters on in situ heat treatment, a change in depth of the T_m, A_{c1} and M_s critical points' isotherms was numerically simulated in dependence on the laser power and laser scanning speed. The isotherms were calculated for a single laser scan with laser scanning speeds of 100, 120 and 140 mm/s and laser powers of 50, 60 and 70 W. The points in Fig. 5 represent the maximum depths of T_m, A_{c1} and M_s isotherms, obtained from the corresponding longitudinal contour plots. It is seen that changes of these parameters mostly influence the depth for the M_s isotherm, Fig. 5. With an increase of the laser power from 50 to 70 W and a decrease of the laser scanning speed from 140 to 100 mm/s, the estimated depth of the M_s isotherm increased by 90–100 μm. In terms of temperature, at an arbitrary selected depth of 200 μm, the same changes of process parameters resulted in an estimated temperature rise by 245 ± 25 °C. This change of the affected depth implies that a selected region will reach higher temperatures during manufacturing. According to [21,25] changes in temperature substantially influenced the amount of reversed austenite in AISI420 steel, and thus also the final properties. The results of the numerical simulation show that the heat affected zone can be quite well controlled by control of the energy input, therefore supporting the concept of a controllable in situ heat treatment during SLM manufacturing. Nevertheless, the concept requires a more systematic experimental verification before it becomes possible to manufacture parts and components with tailored properties at industrial scale.

4. Conclusions

The microstructure of AISI 420 steel manufactured by SLM depends on local thermal cycling conditions, which could be predicted by numerical simulation.

- Thermal cycles modeled for the upper regions suggested that the temperatures were high enough to start diffusional transformation, but an enrichment of the martensite with alloying elements and a very short time at high temperature restricted the martensite decomposition. At the used process parameters, the upper region consisted of martensite with 21 ± 12 vol.% retained austenite and a hardness of 750 HV to the depth of 100–120 μm.
- Microstructures in the inner regions were formed due to carbon partitioning and diffusional processes occurred in situ. At a multiple thermal cycling between M_s and A_{c1} temperatures, a diffusion of carbon segregated at the interphase boundaries during solidification was initiated. Carbon atoms diffused to the most defected regions, the cell boundaries, with a subsequent austenite reversion or growth of the retained austenite. A total amount of 57 ± 8 vol.% austenite and a hardness of 500–550 HV were measured in the inner region.
- Numerical simulation of the thermal history showed good agreement with the experiment, therefore was found plausible to predict the in situ heat treatment occurred in the as built AISI 420 martensitic stainless steel. Based on the experimental results and the numerical analysis, a concept of a controllable in situ heat treatment during SLM to manufacture objects with tailored properties was suggested for future development.

Authors thank colleagues Ru Peng and Sten Johansson at Linköping University of Technology and Anna Medvedeva at Uddeholms AB for the help with EBSD and XRD and National Research Foundation of South Africa, grant 97994, for financial support.

References

[1] T. Wohlers, Wohlers Report: Additive Manufacturing and 3D Printing State of the Industry, Annual Worldwide Progress Report, Wohlers Associates, Fort Collins, 2013.
[2] I. Gibson, D.W. Rosen, B. Stucker, Additive Manufacturing Technologies: Rapid Prototyping to Direct Digital Manufacturing, Springer-Verlag, New York, 2010.
[3] I. Yadroitsev, P. Krakhmalev, I. Yadroitsava, S. Johansson, I. Smurov, Energy input effect on morphology and microstructure of selective laser melting single track from metallic powder, J. Mater. Process. Technol. 213 (2013) 606–613, http://dx.doi.org/10.1016/j.jmatprotec.2012.11.014.
[4] B. Zhang, L. Dembinski, C. Coddet, The study of the laser parameters and environment variables effect on mechanical properties of high compact parts elaborated by selective laser melting 316 L powder, Mater. Sci. Eng. A 584 (2013) 21–31, http://dx.doi.org/10.1016/j.msea.2013.06.055.
[5] J. Sun, Y. Yang, D. Wang, Parametric optimization of selective laser melting for forming Ti6Al4V samples by Taguchi method, Opt. Laser Technol. 49 (2013) 118–124, http://dx.doi.org/10.1016/j.optlastec.2012.12.002.
[6] J.W. Xie, P. Fox, W. O'Neill, C.J. Sutcliffe, Effect of direct laser re-melting processing parameters and scanning strategies on the densification of tool steels, J. Mater. Process. Technol. 170 (2005) 516–523, http://dx.doi.org/10.1016/j.jmatprotec.2005.05.055.
[7] I. Yadroitsev, P. Krakhmalev, I. Yadroitsava, Hierarchical design principles of selective laser melting for high quality metallic objects, Addit. Manufact. 7 (2015) 45–56, http://dx.doi.org/10.1016/j.addma.2014.12.007.
[8] I. Yadroitsev, Selective Laser Melting: Direct Manufacturing of 3D-objects by Selective Laser Melting of Metal Powders, LAP Lambert Academic Publishing AG & Co KG, 2009.
[9] E. Yasa, J.-P. Kruth, Microstructural investigation of selective laser melting 316 L stainless steel parts exposed to laser re-melting, Process. Eng. 19 (2011) 389–395, http://dx.doi.org/10.1016/j.proeng.2011.11.130.
[10] I.A. Roberts, C.J. Wang, R. Esterlein, M. Stanford, D.J. Mynors, A three-dimensional finite element analysis of the temperature field during laser melting of metal powders in additive layer manufacturing, Int. J. Mach. Tools Manuf. 48 (2009) 916–923, http://dx.doi.org/10.1016/j.ijmachtools.2009.07.004.
[11] R. Colaço, R. Vilar, Stabilization of retained austenite in laser surface melted tool steels, Mater. Sci. Eng. A 385 (2004) 123–127, http://dx.doi.org/10.1016/j.msea.2004.06.069.
[12] S.H. Baghjari, S.A.A. Akbari Mousavi, Effects of pulsed Nd:YAG laser welding parameters and subsequent post-weld heat treatment on microstructure and hardness of AISI 420 stainless steel, Mater. Des. 43 (2013) 1–9, http://dx.doi.org/10.1016/j.matdes.2012.06.027.
[13] L.F. Alvarez, C. Garcia, V. Lopez, Continuous cooling transformations in martensitic stainless steels, ISIJ Int. 34 (1994) 516–521, http://dx.doi.org/10.2355/isijinternational.34.516.
[14] G.A. Ravi, X.J. Hao, N. Wain, X. Wu, M.M. Attallah, Direct laser fabrication of three dimensional components using SC420 stainless steel, Mater. Des. 47 (2013) 731–736, http://dx.doi.org/10.1016/j.matdes.2012.12.062.
[15] A. Hussein, L. Hao, C. Yan, R. Everson, Finite element simulation of the temperature and stress fields in single layers built without-support in selective laser melting, Mater. Des. 52 (2013) 638–647, http://dx.doi.org/10.1016/j.matdes.2013.05.070.
[16] P. Krakhmalev, I. Yadroitsava, G. Fredriksson, I. Yadroitsev, Microstructure of SLM manufactured 316 L and 420 grades stainless steel, Proceeding of the RAPDASA 15th Annual International Conference; 2014 November 6–7; Stellenbosch, South Africa 2014, pp. 59–66.
[17] L.E. Murr, E. Martinez, K.N. Amato, S.M. Gaytan, J. Hernandez, D.A. Ramirez, et al., Fabrication of metal and alloy components by additive manufacturing: examples of 3D materials science, J. Mater. Res. Technol. 1 (2012) 42–54, http://dx.doi.org/10.1016/S2238-7854(12)70009-1.
[18] S. Kou, Welding Metallurgy, 2nd ed. Wiley-Interscience, New Jersey, 2003.
[19] K.N. Amato, J. Hernandez, L.E. Murr, E. Martinez, S.M. Gaytan, P.W. Shindo, Comparison of microstructures and properties for a Ni-base superalloy (Alloy 625) fabricated by electron and laser beam melting, J. Mater. Sci. Res. 1 (2012) 3–41, http://dx.doi.org/10.5539/jmsr.v1n2p3.
[20] A.V. Sverdlin, A.R. Ness, The effect of alloying elements on the heat treatment of steel, in: G.E. Totten, M.A.H. Howes (Eds.), Steel Heat Treatment Handbook, Marcel Dekker Inc., New York 2009, pp. 45–93.

[21] L. Yuan, D. Ponge, J. Wittig, P. Choi, J.A. Jiménez, D. Raabe, Nanoscale austenite reversion through partitioning, segregation, and kinetic freezing: example of a ductile 2 GPa Fe–Cr–C steel, Acta Mater. 60 (2012) 2790–2804, http://dx.doi.org/10.1016/j.actamat.2012.01.045.
[22] J. Speer, D.K. Matlock, B.C. DeCooman, J.G. Schroth, Carbon partitioning into austenite after martensite transformation, Acta Mater. 51 (2003) 2611–2622, http://dx.doi.org/10.1016/S1359-6454(03)00059-4.
[23] T. Tsuchiyama, J. Tobata, T. Tao, N. Nakada, S. Takaki, Quenching and partitioning treatment of a low-carbon martensitic stainless steel, Mater. Sci. Eng. A 532 (2012) 585–592, http://dx.doi.org/10.1016/j.msea.2011.10.125.
[24] D.V. Edmonds, K. He, F.C. Rizzo, B.C. DeCooman, D.K. Matlock, J. Speer, Quenching and partitioning martensite — a novel steel heat treatment, Mater. Sci. Eng. A 438–440 (2006) 25–34, http://dx.doi.org/10.1016/j.msea.2006.02.133.
[25] H. Springer, M. Belde, D. Raabe, Bulk combinatorial design of ductile martensitic stainless steels through confined martensite-to-austenite reversion, Mater. Sci. Eng. A 582 (2013) 235–244, http://dx.doi.org/10.1016/j.msea.2013.06.036.